Phenotypes of Vascular Flow Networks

Henrik Ronellenfitsch [1,2,*] and Eleni Katifori[2,†]

[1]*Department of Mathematics, Massachusetts Institute of Technology, Cambridge, Massachusetts 02139, USA*
[2]*Department of Physics and Astronomy, University of Pennsylvania, Philadelphia, Pennsylvania 19104, USA*

Complex distribution networks are pervasive in biology. Examples include nutrient transport in the slime mold *Physarum polycephalum* as well as mammalian and plant venation. Adaptive rules are believed to guide development of these networks and lead to a reticulate, hierarchically nested topology that is both efficient and resilient against perturbations. However, as of yet, no mechanism is known that can generate such networks on all scales. We show how hierarchically organized reticulation can be constructed and maintained through spatially correlated load fluctuations on a particular length scale. We demonstrate that the network topologies generated represent a trade-off between optimizing transport efficiency, construction cost, and damage robustness and identify the Pareto-efficient front that evolution is expected to favor and select for. We show that the typical fluctuation length scale controls the position of the networks on the Pareto front and thus on the spectrum of venation phenotypes.

Complex life would be inconceivable without biological fluid distribution networks such as animal vasculature, plant xylem and phloem, the network of fungal mycelia, or the protoplasmic veins of *Physarum polycephalum*. These networks distribute oxygen and nutrients, remove waste, and serve as long range communication pathways. In mammals, the vast spectrum of venation network phenotypes ranges from predominantly treelike networks, such as the large veins and arteries that service entire organs, to highly reticulated capillaries within the organs, such as in the brain or the liver. In plants, leaf network phenotypic variability even within a single organism can be large, but typically the hierarchical structure and reticulation are roughly conserved. However, within a single family there can be considerable variation [1]. It is therefore natural to ask whether there might be a single developmental mechanism at play that can generate and interpolate between the different archetypes on this phenotypic spectrum of vascular networks. Then, evolution would only need to select for a few parameters in order to tune the network phenotype for its function. Here, we theoretically identify fluctuations during development as such a mechanism and pinpoint networks on a Pareto front possessing optimal trade-offs between hydraulic efficiency, damage resilience, and cost, as evolutionarily desirable.

Many frequently competing factors influence which particular phenotypes are favored by natural selection. Therefore, it is to be expected that the eventual physical form of an organism is shaped by trade-offs between different requirements. Pareto optimality identifies those phenotypes that strike optimal trade-offs between objectives: The Pareto front is the subset of phenotypes where performance at one objective cannot be increased without decreasing performance at another [Fig. 1(b), Ref. [2]]. One can assume that the phenotypes observed in nature are found approximately on some relevant Pareto front because any other trade-off could be improved upon and is therefore evolutionarily selected against, given otherwise fixed conditions [3].

In plants, where a well-preserved fossil record of the venation exists, the fast transitions between reticulate and nonreticulate patterns over evolutionary time are evidence for an easily tunable mechanism generating vascular phenotypes [4,5]. These transitions can also be effected artificially by single gene knockouts [6,7] or small changes in phytohormone concentrations [8]. In the case of animals, often the positions and dimensions of the largest vessels (such as the aorta) are genetically predetermined and fixed. However, smaller vessels are too numerous to be efficiently genetically encoded and are believed to develop in a self-organized fashion [9–11]. The abstract mechanisms governing self-organization of vasculature in plants and animals appear to be universal [12]. For instance, in plant leaves, auxin canalization, involving flow of a chemical morphogen, is believed to guide development of the network pattern [Refs. [13–17], Figs. 1(c) and 1(d)] and in animal vasculature, vessels respond to wall shear stress [10,18–21]. Generically, these mechanisms involve a process that is able to remodel an initial mesh of veins according to the flow of blood (in animals) or cells connected by carrier proteins according to a morphogen (in plants). If the flow is large, vessels adapt by increasing their diameter; unused connections die out. This process has been observed directly in animals [22] and indirectly in plants [23].

Common to the vascular network development of both plants and animals, the dynamics of the hydraulic vessel
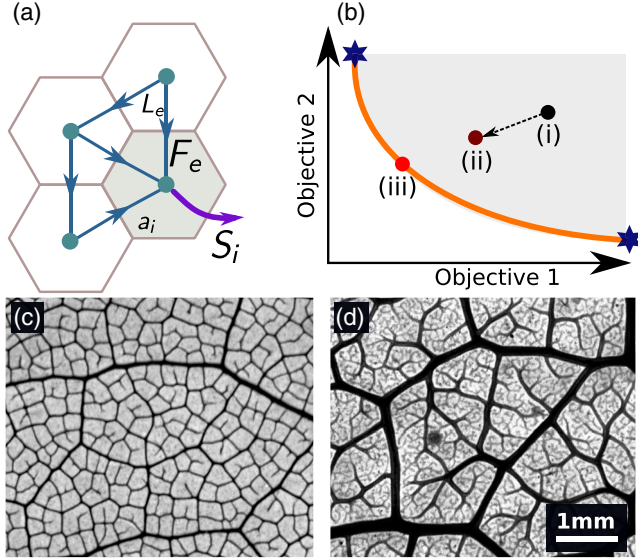
FIG. 1. (a) Network model of liquid transport. Edges e of length L_e carry currents F_e. At each node i, a net current S_i is drawn from the network. The net current S_i models local sources and sinks. (b) The Pareto front (orange) is the set of points out of all possible phenotypes (gray) for which performance cannot be improved at both objectives simultaneously. For any point not on the Pareto front [e.g., (i)] a different point can be found [e.g., (ii)] that has better performance at both objectives. For a point on the Pareto front, like (iii), this is not possible. The endpoints of the Pareto front (stars) are functional archetypes. (c) Leaf veins of *Acer platanoides* near the "reticulate archetype" identified in this Letter. (d) Leaf veins of *Protium dawsonii* show many freely ending veinlets, similar to what is found near the "tree archetype" identified in this Letter.

conductivities K_e can be modeled by an equation of the form [12,21,24–26],

$$\frac{dK_e}{dt} = a\frac{(F_e^2)^\beta}{K_e^{\alpha-1}} - bK_e + ce^{-rt}, \qquad (1)$$

where a, b, c, and r are non-negative adaptation parameters and $\alpha \geq 1$, $\beta > 0$. Often, $\alpha = 1$ and $c = 0$. The dynamical steady states then correspond to different network topologies.

Equation (1) describes a local positive feedback mechanism. Conductivities K_e grow as controlled by the magnitude of a when the current F_e through their vessel is large, and they decay on a characteristic timescale b^{-1} when it is small. The parameter c may be interpreted as the presence of some growth hormone such as vascular endothelial growth factor in the case of mammalian vasculature or background production of auxin transporting proteins in the case of plant leaves [25]. Potential flow is assumed throughout [Fig. 1(a), Supplemental Material [27]]. An explicit time dependence may exist during development, for instance, due to growth of the surrounding tissue or gradual depletion or degradation of the growth factor over a timescale r^{-1} [12].

The generic dynamics of Eq. (1) is characterized by two phases. First, the background production term dominates and produces a homogeneous network. Then, as background production becomes increasingly suppressed due to the exponential decay term, vascular adaptation takes over, generating veins in a hierarchical fashion: thick, main veins first and successively thinner veins later while pruning unused connections, comparable to vascular plexus development [18,22,30,31]. The competition between background production and adaptation leads to hierarchically ordered steady-state networks [12], which are always topological trees [32,33]. While nonhierarchical reticulation can be achieved by postulating new chemicals [34], we now introduce a model of adaptation to fluctuating load that can produce hierarchical reticulation. Such load fluctuations are common in animals (for instance, Ref. [35]) and recent work points toward their existence in plants during development as well [23].

Assuming that the timescale on which fluctuations occur is much smaller than that of adaptation and that fluctuations are characterized by approximately static states between which the system switches quickly, we replace the squared currents in Eq. (1) by a fluctuation average [19,24,36–40],

$$F_e^2 \rightarrow \langle F_e^2 \rangle = \frac{1}{N}\sum_{\text{state } i}(F_e^{(i)})^2. \qquad (2)$$

Here, the vector of fluctuating states $\mathbf{F}^{(i)} = (F_e^{(i)})$ represents the flows in the network for a particular vector of source terms $\mathbf{S}^{(i)} = (S_j^{(i)})$, and the summation performs an ensemble average for a given set of fluctuating states. Then, the dynamical steady states can correspond to minima of optimization models [24,36,37].

We generalize these approaches to include collectively produced fluctuations by using the sources,

$$\frac{S_j^{(i)}}{\hat{S}} = \delta_{j0} - (1-\delta_{j0})f\left(\frac{\|\mathbf{x}_j - \mathbf{x}_i\|}{\sigma}\right), \qquad (3)$$

where $\mathbf{x}_i$ is the position of node i, σ is the scale over which the source strength varies, and $\sum_j S_j^{(i)} = 0$. The total in- and outflow is $\hat{S}$. In the rest of this Letter, we consider Gaussian sources $[f(x) \sim e^{-x^2/2}]$. Other $f(x)$ lead to qualitatively similar results (Supplemental Material [27]). Uncorrelated fluctuations are obtained as $\sigma \rightarrow 0$ and lead to reticulation, but not to significant hierarchical ordering, similar to Figs. 2(a) and 2(f).

We numerically solve a dimensionless form of Eq. (1),

$$\frac{d\tilde{K}_e}{d\tilde{t}} = \langle \tilde{F}_e^2 \rangle^\beta - \tilde{K}_e + \kappa e^{-\tilde{t}/\rho}, \qquad (4)$$

where the tilde denotes dimensionless quantities (Supplemental Material [27]). Following Ref. [12], we
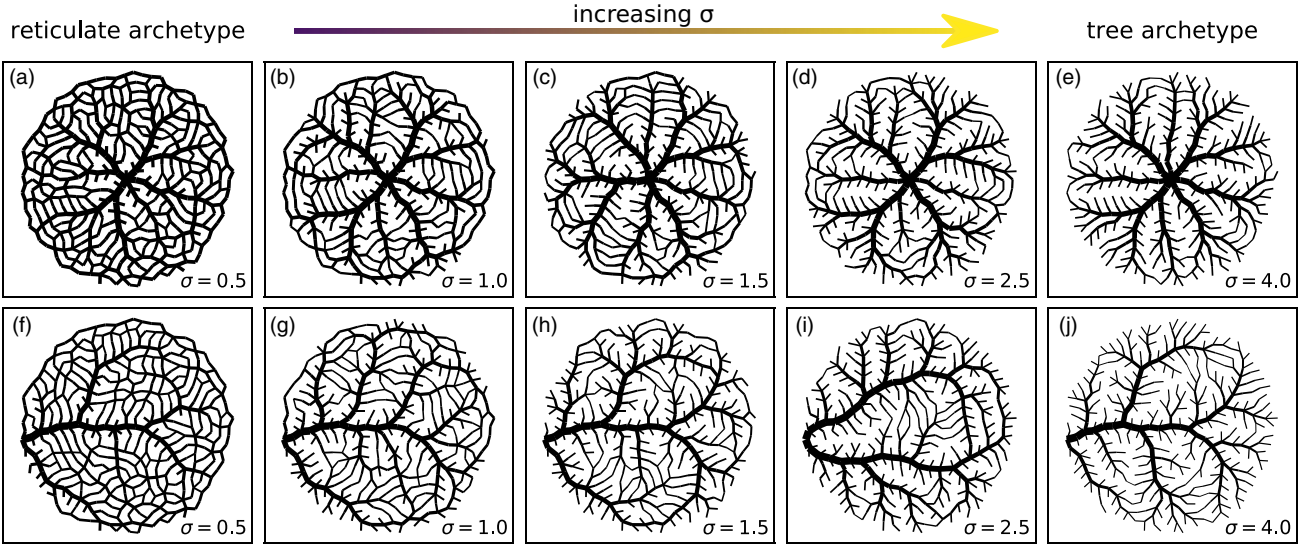
FIG. 2.   The variety of network phenotypes that can be produced with a locally adaptive fluctuating load model. All examples lie on the Pareto front of efficient networks (Fig. 3), thus representing different trade-offs between baseline power dissipation, cost, and damage robustness. The number of loops and thus damage robustness increases to the right, the value of σ increases from 0.5 to 4.0 to the right. The Pareto front corresponds to the whole spectrum of "natural" reticulate networks, from highly hierarchical trees, fragile but cheap, to highly robust reticulate, expensive networks. (a)–(e) The inlet is at the center. (f)–(j) The inlet is at the left side.

set $\alpha = 1$, with other values leading to similar conclusions. The control parameters are the dimensionless background strength $\kappa = (c/a)\hat{S}^{-2\beta}$, the decay timescale $\rho = b/r$, and the fluctuation scale σ. We further fix the nonlinearity at $\beta = 2/3$, which leads to the same steady-state networks as shear-stress adaptation [24]. This value also corresponds to a total network volume constraint [12,37]. All networks start from the same disordered mesh with 445 nodes and 1255 edges. We either place a single inlet at the center of the network, similar to the retina, or at the boundary, similar to a leaf. The conductivities are initialized with random positive numbers, and the scale parameter σ is measured in units of the mean edge length $\hat{L}$.

The interplay between background and decay parameters, fluctuation scale, and boundary conditions leads to a whole spectrum of networks, many of them qualitatively resembling the networks found in dicot and fern leaves, or the vasculature of the retina or the brain. They appear to reproduce well the hierarchical structure seen in real modern plants and animals (Fig. 2). Reticulation in particular is controlled by the fluctuation scale σ. For small $\sigma \ll \hat{L}$, the steady-state networks are highly reticulated, similar to those obtained in Refs. [24,37], and have little hierarchy [Figs. 2(a), 2(b), 2(f), and 2(g)]. As σ becomes comparable to or greater than $\hat{L}$, the networks gradually lose reticulation and gain hierarchical structure, independent of the chosen inlet position [Figs. 2(c)–2(e) and 2(h)–2(j)]. Intuitively, different large-scale sources $\mathbf{S}^{(i)}$ centered at nearby nodes overlap almost completely and effectively act as a single state. Thus, the average is over only a few effective large-scale sources, which leads to

fewer effective fluctuations and therefore less reticulation. We develop a unified framework for arbitrary fluctuating sources by noting that the average flow can be rewritten as the weighted mean (Supplemental Material [27]),

$$\langle F_e^2 \rangle = \frac{1}{N}\sum_i (F_e^{(i)})^2 = \sum_j \rho_j (R_e^{(j)})^2, \qquad (5)$$

where the ρ_j are the eigenvalues of the covariance matrix $(1/N)\sum_k \mathbf{S}^{(k)}(\mathbf{S}^{(k)})^\top$, and the $R_e^{(j)}$ are the flows induced by the associated eigenvectors as sources. For values of $\sigma \gg \hat{L}$, the collective sources themselves become highly correlated to each other, and the source covariance matrix is characterized by only a few dominant eigenvalues, with the vast majority negligibly small, independent of the specific form of $f(x)$ (Supplemental Material [27]). Armed with this model, we proceed to ask which of the network topologies it can produce may be favored by natural selection. We specialize to a single inlet at the center, with other inlet positions leading to qualitatively similar results (Supplemental Material [27]).

Hydraulic efficiency, low cost, and robustness are important but competing requirements, such that we expect that natural selection strikes a trade-off between them. As a measure of network efficiency, we consider the hydraulic power dissipation calculated under nonfluctuating conditions, $E = \sum_e L_e F_e^2/K_e$, where the flows are computed for a single inlet and uniform sinks. The rationale is that, during nominal operation, fluctuations are expected to be small, with large fluctuations to be expected during development. Next, the network cost, $C = \sum_e L_e K_e^\gamma$,
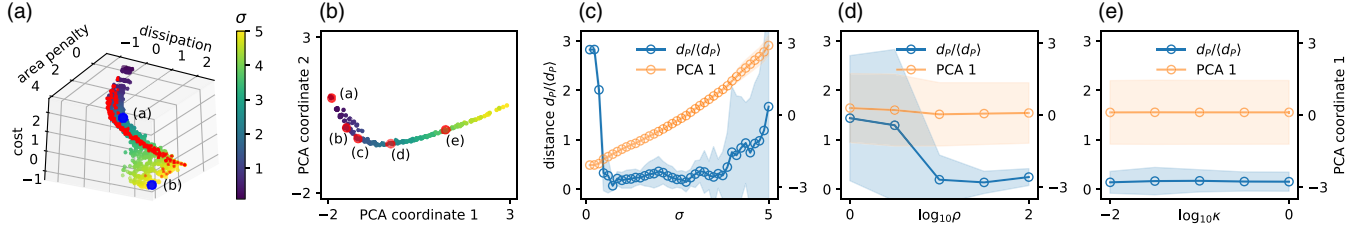
FIG. 3. Geometry of the Pareto front of adaptive distribution networks. We plot the phenotypic space of networks obtained from parameter values $\rho \in \{1, 10, 100\}$, $\kappa \in \{1, 0.1, 0.01\}$, $\sigma \in [0.1, 5]$, $\alpha = 1, \beta = 2/3$ as an example of the phenotypic space that can be reproduced using the model. We calculate the Pareto front for simultaneous minimization of power dissipation, network cost, and percolation penalty. The data were scaled to zero mean and unit variance in each objective. (a) The dataset; colors indicate the value of σ. The Pareto front is in red, and the non-Pareto networks from Fig. 4 are in blue. (b) Principal component analysis (PCA) embedding of the Pareto front from (a). 91% of the variance is encoded in the first PCA coordinate, suggesting that the front is approximately one-dimensional. The first PCA coordinate (PCA 1) approximately parametrizes the Pareto front. Red points correspond to the networks from Figs. 2(a)–2(e). (c) For all combinations (ρ, κ, σ) on the Pareto front P we hold ρ and κ fixed and vary σ. For a wide range of σ, the average distance $d_P(x) = \min_{p \in P} \|x - p\|$ from the Pareto front is well below the mean $\langle d_P \rangle$, suggesting that phenotypes remain close to the Pareto front (blue curve, shaded region is one standard deviation over combinations of ρ, κ). Varying σ moves linearly along the Pareto front parametrized by PCA 1 (orange curve). Thus, σ approximately parametrizes the Pareto front. Similarly varying ρ (d) or κ (e) while holding the other parameters fixed may lead to phenotypes close to the Pareto front for large ρ and all κ, but the position on the front PCA 1 is random. Thus, ρ and κ cannot be used to parametrize the Pareto front.

where $\gamma < 1$ models an economy of scale, measures the amount of material investment that goes into constructing the network. This should be minimized by any organism that efficiently uses its resources. We set $\gamma = 1/2$, which corresponds to a cost proportional to the total vessel volume or, equivalently, total material used to construct the network. Finally, we consider a percolation penalty as a measure of network robustness, quantifying the cost of losing part of the vasculature to damage. We choose the expected fraction of perfused area lost upon removing an edge, $\hat{A} = (1/N_e) \sum_e A_e / A_{\text{tot}}$, where A_e is the area of the network that becomes disconnected from the source upon removal of edge e, A_{tot} is the total area of the network, and N_e is the number of edges. Efficient network phenotypes must minimize the cost C, the power dissipation E, and the percolation penalty A.

Observations of real networks, for instance, in leaves, reveal that many treelike components exist and that they are important for transport [41]. This means that, although the percolation penalty is minimized, it is not expected to be perfectly zero. Except for very small $\sigma \ll \hat{L}$ and very large $\sigma \gg \hat{L}$, network phenotypes obtained from our model generically exhibit these small treelike components within loops (Fig. 2).

We scanned a portion of the parameter space and computed the three network measures for a dataset of steady states of the adaptation dynamics. The steady-state networks form a dense cloud in the space of network measures [Fig. 3(a)]. Computing the Pareto front using the algorithm from Ref. [42] and analyzing its geometry using PCA reveals an approximately one-dimensional line of points [Fig. 3(b), Supplemental Material [27]]. Fixing ρ and κ, the parameter σ approximately parametrizes networks on the Pareto front [Figs. 3(c)–3(e)], such that σ can

be used to tune optimal trade-offs between the three objectives. The endpoints of the Pareto front correspond to functional archetypes [3], on one end low-cost, fragile, and nonreticulate high-dissipation networks ($\sigma \gg \hat{L}$, tree archetype), and on the other end high-cost, robust, and fully reticulate low-dissipation networks ($\sigma \ll \hat{L}$, reticulate archetype) (Figs. 2 and 3). For small $\sigma \ll \hat{L}$, most networks lie close to the front, whereas for large $\sigma \gg \hat{L}$, there is greater variability, and many networks lie far from the front [Figs. 3(a) and 3(b)]. Defining a distance $d_P(x) = \min_{p \in P} \|x - p\|$ from the Pareto front P and rescaling all network measures to have unit variance and mean zero so as to bring them to the same scale, the mean distance from the front is $\langle d_P \rangle \approx 0.24$. The Pareto front comprises 14% of all networks. From the remaining ones, 70% lie closer than average to the front and 30% lie further than average from the front. Tuning κ by itself without fixing the other parameters has little effect on the distance of networks from the Pareto front. However, $\rho \gtrsim 10$ or $0.5 \lesssim \sigma \lesssim 3$ can generically drive the network phenotypes close to the front (Supplemental Material [27]). Non-Pareto optimal phenotypes often show branching with parallel instead of roughly perpendicular veins (Fig. 4). Open, nonhierarchical venation patterns similar to those of some networks off the Pareto front can be found in the leaves of the evolutionarily archaic *Ginkgo biloba* tree [Fig. 4(b), Refs. [43,44]].

We have shown that a simple, easily tunable mechanism is able to produce an entire spectrum of phenotypic variation in vascular networks. The shape of networks on this spectrum can be rationalized by the interplay between flow fluctuations affecting developmental processes and natural selection of parameters that lead to phenotypes on a Pareto front of optimal trade-offs between efficiency, cost, and resilience. The networks on the Pareto
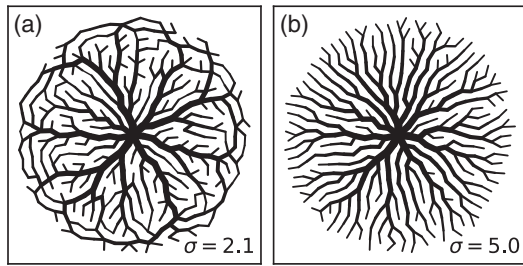
FIG. 4. Network phenotypes not lying on the Pareto front show less hierarchical organization for the same amount of reticulation than their Pareto optimal counterparts. In both networks, $\kappa = 1.0$, $\rho = 1.0$. (a) $E = 6.0$, $A = 0.48$, $C = 47.0$. (b) $E = 10.8$, $A = 7.73$, $C = 32.8$.

front are reminiscent of modern natural leaf or animal vasculature, suggesting that natural networks may be subject to the trade-offs we consider. Networks away from the Pareto front generically exhibit less hierarchical organization and less resemblance to modern plants and animals. Out of the three control parameters of our model, only the fluctuation scale is highly correlated to the position on the Pareto front and thus to the position on the spectrum of vascular networks. This could allow natural selection to more easily adjust for a given needed functionality, but also to reuse the same genetic pathway to construct networks with different functionality in the same organism. Beyond biology, engineered transport networks such as electrical power grids are often subject to similar trade-offs, such that we expect that our analysis will be useful here as well.

[*]henrikr@mit.edu

[†]katifori@sas.upenn.edu

[1] H. Ronellenfitsch, J. Lasser, D. C. Daly, and E. Katifori, Topological phenotypes constitute a new dimension in the phenotypic space of leaf venation networks, PLoS Comput. Biol. **11**, e1004680 (2015).

[2] K. Miettinen, *Nonlinear Multiobjective Optimization*, International Series in Operations Research & Management Science (Springer, New York, 1999).

[3] O. Shoval, H. Sheftel, G. Shinar, Y. Hart, O. Ramote, A. Mayo, E. Dekel, K. Kavanagh, and U. Alon, Evolutionary trade-offs, Pareto optimality, and the geometry of phenotype space, Science **336**, 1157 (2012).

[4] T. J. Givnish, J. C. Pires, S. W. Graham, M. A. McPherson, L. M. Prince, T. B. Patterson, H. S. Rai, E. H. Roalson, T. M. Evans, W. J. Hahn, K. C. Millam, A. W. Meerow,

M. Molvray, P. J. Kores, H. E. O'Brien, J. C. Hall, W. J. Kress, and K. J. Sytsma, Repeated evolution of net venation and fleshy fruits among monocots in shaded habitats confirms a priori predictions: Evidence from an ndhF phylogeny, Proc. R. Soc. B **272**, 1481 (2005).

[5] B. Blonder, B. G. Baldwin, B. J. Enquist, and R. H. Robichaux, Variation and macroevolution in leaf functional traits in the Hawaiian silversword alliance (Asteraceae), J. Ecol. **104**, 219 (2016).

[6] Q. J. Steynen and E. A. Schultz, The FORKED genes are essential for distal vein meeting in Arabidopsis. Development **130**, 4695 (2003).

[7] F. Carland and T. Nelson, CVP2- and CVL1-mediated phosphoinositide signaling as a regulator of the ARF GAP SFC/VAN3 in establishment of foliar vein patterns, Plant J. **59**, 895 (2009).

[8] T. Berleth, J. Mattsson, and C. S. Hardtke, Vascular continuity and auxin signals, Trends Plant Sci. **5**, 387 (2000).

[9] F. le Noble, V. Fleury, A. Pries, P. Corvol, A. Eichmann, and R. S. Reneman, Control of arterial branching morphogenesis in embryogenesis: Go with the flow. Cardiovasc. Res. **65**, 619 (2005).

[10] H. Kurz, Physiology of angiogenesis, J. Neuro-Oncol. **50**, 17 (2001).

[11] T.-H. Nguyen, A. Eichmann, F. Le Noble, and V. Fleury, Dynamics of vascular branching morphogenesis: The effect of blood and tissue flow, Phys. Rev. E **73**, 061907 (2006).

[12] H. Ronellenfitsch and E. Katifori, Global Optimization, Local Adaptation, and the Role of Growth in Distribution Networks, Phys. Rev. Lett. **117**, 138301 (2016).

[13] R. S. Smith and E. M. Bayer, Auxin transport-feedback models of patterning in plants, Plant, Cell Environ. **32**, 1258 (2009).

[14] E. Scarpella, Control of leaf vascular patterning by polar auxin transport, Genes Dev. **20**, 1015 (2006).

[15] C. Verna, M. G. Sawchuk, N. M. Linh, and E. Scarpella, Control of vein network topology by auxin transport, BMC Biol. **13**, 94 (2015).

[16] F. G. Feugier, A. Mochizuki, and Y. Iwasa, Self-organization of the vascular system in plant leaves: Inter-dependent dynamics of auxin flux and carrier proteins, J. Theor. Biol. **236**, 366 (2005).

[17] C. Feller, E. Farcot, and C. Mazza, Self-organization of plant vascular systems: Claims and counter-claims about the flux-based auxin transport model, PLoS One **10**, e0118238 (2015).

[18] A. Eichmann, L. Yuan, D. Moyon, F. Lenoble, L. Pardanaud, and C. Breant, Vascular development: From precursor cells to branched arterial and venous networks, Int. J. Dev. Biol. **49**, 259 (2005).

[19] D. Hu, D. Cai, and A. V. Rangan, Blood vessel adaptation with fluctuations in capillary flow distribution, PLoS One **7**, e45444 (2012).

[20] M. Scianna, C. G. Bell, and L. Preziosi, A review of mathematical models for the formation of vascular networks. J. Theor. Biol. **333**, 174 (2013).

[21] W. J. Hacking, E. VanBavel, and J. A. E. Spaan, Shear stress is not sufficient to control growth of vascular networks: A model study, Am. J. Physiol. **270**, H364 (1996).

[22] Q. Chen, L. Jiang, C. Li, D. Hu, J.-W. Bu, D. Cai, and J.-L. Du, Haemodynamics-driven developmental pruning of brain vasculature in zebrafish, PLoS Biol. **10,** e1001374 (2012).

[23] D. Marcos and T. Berleth, Dynamic auxin transport patterns preceding vein formation revealed by live-imaging of Arabidopsis leaf primordia, Front. Plant Sci. **5,** 235 (2014).

[24] D. Hu and D. Cai, Adaptation and Optimization of Biological Transport Networks, Phys. Rev. Lett. **111,** 138701 (2013).

[25] A.-G. Rolland-Lagan and P. Prusinkiewicz, Reviewing models of auxin canalization in the context of leaf vein pattern formation in Arabidopsis, Plant J. **44,** 854 (2005).

[26] K. van Berkel, R. J. de Boer, B. Scheres, and K. ten Tusscher, Polar auxin transport: Models and mechanisms, Development **140,** 2253 (2013).

[27] See Supplemental Material at http://link.aps.org/supplemental/10.1103/PhysRevLett.123.248101 for detailed calculations and additional results for other network topologies, source functions, and parameter values, which includes Refs. [28,29].

[28] J. J. Blakeslee, W. A. Peer, and A. S. Murphy, Auxin transport, Curr. Opin. Plant Biol. **8,** 494 (2005).

[29] E. M. Kramer and M. J. Bennett, Auxin transport: A field in flux, Trends Plant Sci. **11,** 382 (2006).

[30] V. Fleury and M. Unbekandt, The textural aspects of vessel formation during embryo development and their relation to gastrulation movements, Organogenesis **3,** 49 (2007).

[31] M. Fruttiger, Development of the retinal vasculature, Angiogenesis **10,** 77 (2007).

[32] M. Bernot, V. Caselles, and J.-M. Morel, *Optimal Transportation Networks*, Lecture Notes in Mathematics Vol. 1955 (Springer, Berlin, 2009).

[33] J. R. Banavar, F. Colaiori, A. Flammini, A. Maritan, and A. Rinaldo, Topology of the Fittest Transportation Network, Phys. Rev. Lett. **84,** 4745 (2000).

[34] F. G. Feugier and Y. Iwasa, How canalization can make loops: A new model of reticulated leaf vascular pattern formation, J. Theor. Biol. **243,** 235 (2006).

[35] P. J. Drew, A. Y. Shih, and D. Kleinfeld, Fluctuating and sensory-induced vasodynamics in rodent cortex extend arteriole capacity, Proc. Natl. Acad. Sci. U.S.A. **108,** 8473 (2011).

[36] F. Corson, Fluctuations and Redundancy in Optimal Transport Networks, Phys. Rev. Lett. **104,** 048703 (2010).

[37] E. Katifori, G. J. Szöllősi, and M. O. Magnasco, Damage and Fluctuations Induce Loops in Optimal Transport Networks, Phys. Rev. Lett. **104,** 048704 (2010).

[38] H. Ronellenfitsch, J. Dunkel, and M. Wilczek, Optimal Noise-Canceling Networks, Phys. Rev. Lett. **121,** 208301 (2018).

[39] J. Gräwer, C. D. Modes, M. O. Magnasco, and E. Katifori, Structural self-assembly and avalanchelike dynamics in locally adaptive networks, Phys. Rev. E **92,** 012801 (2015).

[40] E. Andreas Martens and K. Klemm, Transitions from trees to cycles in adaptive flow networks, Front. Phys. **5,** 62 (2017).

[41] L. Fiorin, T. J. Brodribb, and T. Anfodillo, Transport efficiency through uniformity: Organization of veins and stomata in angiosperm leaves, New Phytol. **209,** 216 (2016).

[42] M. Geilen and T. Basten, A calculator for Pareto points, in *2007 Design, Automation & Test in Europe Conference & Exhibition* (IEEE, New York, 2007), Vol. 2, pp. 1–6, https://ieeexplore.ieee.org/document/4211810.

[43] Z. Zhou and S. Zheng, The missing link in Ginkgo evolution, Nature (London) **423,** 821 (2003).

[44] V. Martin Dörken, Morphology, anatomy and vasculature in leaves of Ginkgo biloba L. (Ginkgoaceae, Ginkgoales) under functional and evolutionary aspects, Feddes Repertorium **124,** 80 (2014).